HHS Public Access

Author manuscript

Curr Biol. Author manuscript; available in PMC 2022 September 27.

Published in final edited form as:

Curr Biol. 2021 September 27; 31(18): 4139–4147.e6. doi:10.1016/j.cub.2021.06.081.

Striatal low-threshold spiking interneurons locally gate dopamine

Elizabeth N. Holly[1,*], **M. Felicia Davatolhagh**[1,2], **Rodrigo A. España**[3], **Marc V. Fuccillo**[1,*,+]

[1]Department of Neuroscience University of Pennsylvania, Philadelphia, PA, USA

[2]Neuroscience Graduate Group, Perelman School of Medicine, University of Pennsylvania, Philadelphia, PA, USA

[3]Department of Neurobiology and Anatomy, Drexel University College of Medicine, Philadelphia, PA, USA

SUMMARY

The dorsomedial striatum (DMS) is a central hub supporting goal-directed learning and motor performance. Recent evidence has revealed unexpected roles for local inhibitory GABAergic networks in modulating striatal output and behavior[1]. The sparse low-threshold spiking interneuron subtype (LTSI), which exhibits robust reward-circumscribed population activity, is a bi-directional regulator of initial goal-directed learning[2]. Striatal dopamine signaling is a central reward-related neuromodulatory system mediating goal-directed action and performance, serving as a teaching signal[3], facilitating synaptic plasticity[4] and invigorating motor behaviors[5]. Given the dynamic modulation of LTSIs during goal-directed behavior, we hypothesized they could provide a novel GABAergic mechanism of local striatal dopaminergic regulation to shape early learning. We provide anatomical evidence for close proximation of LTSI terminals and dopaminergic processes in striatum, suggesting LTSIs directly control dopaminergic axon activity. Using *in vitro* fast scan cyclic voltammetry, we demonstrate LTSIs directly attenuate optogenetically-evoked dopamine via $GABA_B$ receptor signaling. *In vivo*, $GRAB_{DA}$ dopamine sensor imaging shows that LTSIs strongly modulate striatal dopamine dynamics during operant learning, while pharmacological stabilization of dopamine via intra-striatal aripiprazole microinjection suppresses

*co-corresponding authors.
+lead contact
Twitter handles: @ENHolly and @Fuccillomarc

AUTHOR CONTRIBUTIONS

Conceptualization, ENH and MVF; Methodology ENH, RAE, MVF; Formal Analysis ENH; Investigation ENH, MFD; Writing - Original Draft, ENH; Writing - Review and Editing, ENH, MFD, RAE, MVF; Funding Acquisition, ENH, MVF.

DECLARATION OF INTERESTS

The authors declare no competing interests.

INCLUSION AND DIVERSITY

One or more of the authors of this paper self-identifies as an underrepresented ethnic minority in science. One or more of the authors of this paper self-identifies as living with a disability. One or more of the authors of this paper received support from a program designed to increase minority representation in science. While citing references scientifically relevant for this work, we also actively worked to promote gender balance in our reference list.

the effects of LTSI inhibition on learning. Together, these results uncover an unexpected function for LTSIs in gating striatal dopamine to facilitate goal-directed learning.

eTOC Blurb

Low-threshold spiking interneurons (LTSIs) in the dorsomedial striatum facilitate goal-directed learning. Here, Holly *et al.* suggest that it is LTSI interactions with dopamine that facilitates goal-directed learning, demonstrating that LTSIs locally and directly modulate striatal dopamine both in slice and *in vivo* during operant task acquisition.

RESULTS AND DISCUSSION

LTSIs locally and directly attenuate dopamine via $GABA_B$ receptor signaling

To probe for initial evidence of LTSI-dopamine interactions, we performed *in vivo* microdialysis of extracellular striatal dopamine. Somatostatin-IRES-Cre (SST-Cre) mice were used for selective manipulation of striatal LTSIs[2]. While LTSIs can be identified by a range of markers such as SST, nitric oxide synthase, and neuropeptide Y, we have previously validated that most (>90%) SST-Cre+ cells from this mouse line are indeed SST+, and these SST-Cre+ cells exhibit electrophysiological properties characteristic of LTSIs[2]. Inhibition of striatal LTSIs via Cre-dependent overexpression of Kir2.1, an inwardly rectifying potassium channel that regulates cell-intrinsic excitability[6], significantly augmented extracellular dopamine evoked by a low dose of amphetamine (Figure S1A). While this evidence supports an interaction between LTSIs and dopaminergic transmission, multiple potential mechanisms could generate these effects: (1) direct dopamine axon inhibition, (2) disinhibition of local cholinergic interneurons (ChINs), which strongly regulate dopamine[7–12], and/or (3) disinhibition of local spiny projection neurons (SPNs), which can regulate dopamine via recurrent circuitry projecting back to the midbrain[13].

We were intrigued by the possibility that LTSIs could directly innervate dopamine axons to locally regulate release. To explore this possibility, we injected $SST^{Flp/+}$;$DAT^{Cre/+}$ mice with Flp-dependent Synaptophysin-mRuby to label LTSI terminals and Cre-dependent Synaptophysin-GFP to label dopaminergic terminals, as well as performed immunohistochemistry for tyrosine hydroxylase (TH) to demarcate the entirety of the dopamine neuron processes (Figure 1A). We observed synaptophysin-labeled LTSI synapses that co-localized with tyrosine hydroxylase immunoreactive fibers in close proximity to synaptophysin-labeled dopaminergic terminals (Figure 1A–C), supportive of potential direct axo-axonal interactions between LTSI and dopamine neuron processes.

We directly probed for functional interactions between LTSIs and dopamine axons with *ex vivo* fast scan cyclic voltammetry. Using $SST^{Flp/+}$;$DAT^{Cre/+}$ mice, we gained selective control of these two populations via Flp- and Cre-dependent viruses. Potential contributions of ChINs were eliminated by optogenetically stimulating dopamine terminals expressing Cre-dependent channelrhodopsin and performing all experiments in the presence of antagonists for cholinergic nicotinic β2 (DHβE) and muscarinic (scopolamine) receptors. ChINs predominately regulate dopamine via nicotinic β2 subunits[9,14], and β2 antagonism disrupts ChIN-dopamine interactions to a similar degree as broad nicotinic antagonists

such as mecamylamine[14]. We eliminated downstream effects of LTSI-SPN interactions by performing experiments in acute coronal striatal slices, which disrupts SPN projections to the midbrain. LTSIs are tonically active in slice[15], so we first tested the effects of LTSI inhibition via Flp-dependent halorhodopsin on dopamine optically evoked by Cre-dependent channelrhodopsin (oDA; Figure 1D–F). Halorhodopsin-mediated LTSI inhibition augmented oDA when dopamine axons were stimulated in the middle of both 4s (mirroring prior *in vivo* manipulations[2]) and briefer 400ms windows of LTSI inhibition (Figure 1F, 'Mid'). We additionally tested the temporal precision of LTSI-dopamine control, noting a similar oDA augmentation when LTSI inhibition terminated 500ms prior to dopamine axon stimulation (Figure 1F, 'Delayed'). This prolonged effect of LTSI inhibition suggests longer lasting metabotropic as opposed to ionotropic mechanisms of regulation.

Growing evidence points to a clear role of tonic GABA signaling locally modulating dopamine release in the striatum via both $GABA_A$ and $GABA_B$ transmission[16–18]. As LTSIs are tonically active in acute striatal slices[15], they are a compelling candidate source for this modulatory GABAergic tone. To mechanistically probe how LTSIs gate oDA, we next employed chemogenetic activation of Flp-dependent hM3D-Gq to increase LTSI tonic firing (Figure 1G–I). Supporting a bidirectional role of LTSI-dopamine interactions, increasing LTSI activity suppressed oDA. Activation of both $GABA_A$[16–18] and $GABA_B$[16,17] (Figure S1B) can suppress evoked dopamine in slice. The suppression we observed consequent to LTSI excitation was not affected by $GABA_A$ antagonism (Figure 1K). In contrast, $GABA_B$ antagonism inhibited the LTSI excitation-induced oDA suppression (Figure 1L), and prevented oDA suppression when applied prior to LTSI excitation (Figure 1M). Together, these experiments suggest that LTSIs gate striatal dopamine release via $GABA_B$ locally and directly, independently of ChIN- or striatal loop-mediated mechanisms.

LTSI inhibition amplifies dopamine signaling and accelerates operant learning

We next interrogated whether LTSI inhibition also alters dopamine signaling *in vivo* during learning. As a population, LTSIs exhibit robust reward-circumscribed activity that is downmodulated across operant learning, and selective optogenetic inhibition during reward retrieval accelerates task acquisition[2]. Given the dynamic modulation of LTSIs *in vivo* and LTSI modulation of oDA in slice, we hypothesized LTSI inhibition would amplify dopamine during operant learning, particularly in response to rewards prior to task acquisition. To monitor striatal dopamine with sub-second resolution, we imaged the GRAB-DA (GRAB-DA2m) dopamine sensor[19] as $SST^{Cre/+}$ mice acquired a self-initiated operant task[2] (Figure 2A–C). We modeled learning as a sigmoidal function of accuracy[20–23], with the active learning period defined as trials where accuracy rapidly increased (see Methods; Figures 2D, S1C). Replicating and extending our prior work[2], we show that LTSI inhibition via Cre-dependent Kir2.1 overexpression in the DMS accelerates learning compared to Cre-dependent mRuby expressing controls (Figure 2E, Figure S1C), with increased accuracy during the period of active learning (Figure 2F) driven by fewer omissions (Figure S1F) but not incorrect responses (Figure S1G). Notably, LTSI inhibition did not alter the duration of the pre-learning period, but rather the rate at which learning occurred (Figure 2E). While LTSI inhibition increased response rate and decreased lever press latency, initiation and reward retrieval latencies were unaffected (Figure S1H–K). These selective increases

in accuracy, response rate, and lever press latency with LTSI inhibition point to an enhancement in learning as opposed to generalized increase in locomotor activity[24].

Consistent with our microdialysis and FSCV results, LTSI inhibition amplified the overall height and frequency of GRAB-DA dopamine peak events (Figure S1E). We next explored whether LTSI inhibition selectively affected dopamine signals during discrete behavioral events or stages of learning. The operant task structure allows for dissection of discrete signals in response to trial initiation, lever press, reward retrieval, and within the inter-trial interval (Figure 2C). By aligning dopamine signals to these specific behavioral events (Figure 2G–I, S1L), we revealed dynamic changes in dopamine signals across learning stages.

In pre-learning trials (those on the sigmoidal function prior to the rapid increase in accuracy), we observed transient dopamine signals circumscribed to the correct lever press and retrieval of the reward (Figure 2G). As learning proceeded, the dopamine signal connected to the correct lever press grew, while the dopamine signal aligned to the reward retrieval decreased (Figure 2G). LTSI inhibition did not alter the general progression of dopamine signals across learning, but rather augmented select signals at specific learning stages (Figure 2H,I). Prior to learning, LTSI inhibition selectively amplified dopamine signals during reward retrieval, while transients during other behavioral epochs remained unaffected. During active learning, LTSI inhibition amplified reward-related transients, while after task acquisition LTSI inhibition selectively amplified choice-related dopamine signals (Figure 2H,I). Initiation and ITI-related signals decreasing below baseline are likely biologically relevant as opposed to artifacts of recording time, as signals aligned to minute timestamps as opposed to behavioral events did not decrease across the session (Figure S1M).

To gain further insight into how movement direction is integrated into these dopamine signals, we performed separate analyses of mice trained to press the lever contralateral (Figure S2A–E) or ipsilateral (Figure S2F–J) to their photometry implant. Consistent with prior reports[25,26], we observed stronger striatal dopamine signals during contralateral movements compared to ipsilateral movements. Dopamine signals grew across learning as mice approached and pressed the lever contralateral to their photometry implant (Figure S2A–C). In contrast, in mice trained to press the lever ipsilateral to the photometry implant dopamine signals did not peak until after the lever press, as mice were initiating a contralateral movement back towards the reward magazine (Figure S2F–H). LTSI inhibition amplified dopamine signals in response to contralateral movement towards the magazine only in early stages of learning (Figure S2I,J), while contralateral movements towards the lever were amplified in later stages of learning (Figure S2D,E).

Intra-striatal dopamine D2 partial agonism prevents the effects of LTSI inhibition on learning

Overall, we find that as mice learn a goal-directed task, dopamine signals shift from reward-oriented to contralateral movement-oriented. Furthermore, LTSI inhibition amplifies dopamine signals in response to reward, particularly in early learning, which may contribute to accelerated task acquisition. To test this, we combined viral LTSI manipulation with

local microinjection of aripiprazole, a dopamine D2 partial agonist. Aripiprazole increases dopamine synthesis when basal dopamine is low, while decreasing dopamine synthesis when basal dopamine is higher[27,28]. We hypothesized aripiprazole would stabilize striatal dopamine levels between LTSI-inhibited and LTSI-control mice, thereby suppressing an enhancement in learning rate mediated by LTSI inhibition. Microinjection of 100ng aripiprazole into the DMS prior to operant acquisition sessions (Figure 3A,B) blocked the effects of LTSI inhibition on operant learning rate (Figure 3C,S3). Importantly, these aripiprazole doses did not produce overt effects on overall motor activity as measured by operant task latencies (Figure S3D–F) and rate of lever pressing (not shown) or as separately recorded in an open field (Figure 3D). However, it is important to note that it is unclear if these effects are due to differential alterations in dopamine release from the presynaptic terminals, or postsynaptic modulation of SPNs and/or ChINs, both of which are also under LTSI control.

Discussion

Our data demonstrate that LTSIs provide a novel mechanism for local modulation of dopaminergic signaling, acting to gate synaptically released dopamine. This dynamic regulation occurs both in slice and *in vivo*, and in part underlies the effects of LTSI manipulations on operant learning. By directly inhibiting dopaminergic processes, LTSIs locally modulate dopamine efflux by suppressing dopamine release evoked by dopamine cell body activity or other local modulatory mechanisms in the striatum. Over the course of operant acquisition, both overall and reward-circumscribed LTSI population activity is downmodulated[2], and the present data indicate that removing this inhibitory brake on reward-associated dopaminergic activity is an important driver of early learning. As learning proceeds and dopamine signals shift forward towards the choice period, the effect of LTSI inhibition on dopaminergic signaling is diminished. We also note a significant amplification of choice-associated dopamine signals with LTSI inhibition in the post-learning stage. We suggest this arises from small choice-aligned decreases in LTSI activity that were obscured in our prior population analysis that did not distinguish choice laterality.

Multiple mechanisms could support LTSI modulation of dopamine: (1) direct dopamine axon inhibition, (2) disinhibition of local cholinergic interneurons (ChINs), which strongly regulate dopamine[7–12], and/or (3) disinhibition of local spiny projection neurons (SPNs), which can regulate dopamine via connectivity to the midbrain[13]. Here, not only do we provide anatomical evidence that suggests LTSIs directly innervate dopaminergic axons, but we were also able to demonstrate that LTSI inhibition can amplify dopamine independent of ChIN or SPN disinhibition. Our FSCV experiments were performed in the presence of cholinergic antagonists, blocking any potential effects of ChIN disinhibition, and in acute coronal slices, which severs the potential connectivity between SPNs and dopaminergic cell bodies in the midbrain. It is further unlikely that LTSI disinhibition of other local GABAergic interneurons mediates this effect. Most importantly, GABA inhibits rather than amplifies striatal dopamine release[16–18], so LTSI inhibition or disinhibition of other GABAergic interneurons would have the opposite effect from what was observed. In addition to LTSIs, two other sparse populations of striatal GABAergic interneurons have spontaneous activity in slice: a subset of tyrosine hydroxylase interneurons (THINs[1,29]),

and the recently described spontaneously active bursty interneuron (SABI[30]). While THINs potently inhibit LTSIs, this connectivity is not reciprocal[29]. Therefore, the effects of LTSI modulation on dopamine are unlikely to be a result of THIN or SABI disinhibition, although it is formally possible that these other sparse populations of GABAergic interneurons could also contribute to the tonic GABA tone. However, while our anatomical and FSCV data support a direct $GABA_B$ mechanism by which LTSIs modulate dopamine *in vitro*, it remains unclear if this mechanism underlies the effects of LTSI inhibition on dopamine signals *in vivo*, where other mechanisms such as ChIN or SPN disinhibition cannot be excluded.

Due to the biophysical constraints of lengthy and highly-branched dopamine axons, local regulatory mechanisms are essential in further refining striatal dopamine output[31]. Recent work highlights a behaviorally relevant dissociation between dopaminergic cell body activity and local dopamine concentrations in the striatum[32–34]. Importantly, local microcircuitry directly gates dopamine at the terminals, regulating the magnitude, spread, timing, and duration of dopamine signals[7,35,36], allowing for striatal subregions supporting diverse behavioral functions to tune dopamine release to support local needs[37]. By virtue of their unique reward-associated modulation[2], LTSIs are ideally situated to control the timing and magnitude of dopamine signals during learning. In addition to directly gating striatal dopamine, LTSIs further participate in this local modulatory microenvironment through strong inhibitory control over ChINs[38–41], which also directly and strongly regulate striatal dopamine[8–12]. As both LTSIs and ChINs are dynamically modulated by discrete components of reward learning and performance, future work should delineate how these interneurons work in concert to shape dopamine signals during ongoing goal-directed behavior.

In light of our data, it is also worth reconsidering whether known regulators of LTSI activity could thereby indirectly influence local striatal DA regulation. LTSIs receive substantial excitatory input from medial orbital frontal cortex and anterior cingulate cortex[42], and are under local inhibitory regulation by tyrosine hydroxylase-positive interneurons (ThINs), which are strongly recruited by parafasicular thalamic inputs to the DMS[29]. Finally, serotonin, which is abundantly expressed in striatum and impacts reward learning and motivation, has been shown to hyperpolarize LTSIs, perhaps creating a feedback pathway between these two neuromodulatory pathways[43].

Corticostriatal connectivity drives action selection and performance, and plasticity in these circuits is critical for motor control and learning. We suggest that LTSIs act as a coordinator of corticostriatal plasticity, owing to their combined local modulation of dopamine and dendritic inhibitory functions[38]. During early learning, dopamine solidifies corticostriatal eligibility traces, facilitating long term plasticity[44] and strengthening the association between action selection and outcome. As we demonstrate, striatal LTSI activity can gate this dopaminergic facilitation, accelerating operant acquisition. As learning progresses, LTSI amplification of dopamine signaling may invigorate movement through direct involvement in action selection or execution[25]. In parallel to local dopamine modulation, LTSIs control the flow of cortical input to the striatum via state-dependent feedforward inhibitory actions on SPN distal dendrites[38,45]. Removing the LTSI brake on both striatal dopamine and distal

dendritic compartments in a coordinated manner likely facilitates synaptic plasticity, thereby strengthening action-outcome associations and promoting future goal-directed behavior.

STAR Methods

RESOURCE AVAILABILITY

Lead Contact—Further information and requests for resources should be directed to and will be fulfilled by the lead contact Marc Fuccillo (fuccillo@pennmedicine.upenn.edu).

Materials availability—This study did not generate new unique reagents.

Data and code availability—All data reported in this paper will be shared by the lead contact upon request. All original code has been deposited in the Fuccillo-lab github site and is publicly available as of the date of this publication. The DOI is listed in the Key Resource table. Any additional information required to reanalyze the data reported in this paper is available from the lead contact upon request.

EXPERIMENTAL MODEL AND SUBJECT DETAILS

Animals—All mice (SST-IRES-Cre, Jackson stock number 013044, RRID:IMSR_JAX:013044; SST-IRES-Flp, Jackson stock number 028579, RRID:IMSR_JAX:028579; DAT-IRES-Cre, Jackson stock number 006660, RRID:ISMR_JAX:006660) were bred in house. Prior to experimental manipulation, mice were group housed with littermates on a 12:12 light-dark cycle and provided *ad libitum* food and water. Unless otherwise noted, all experiments were conducted on naïve adult male mice, which were randomly assigned to experimental groups. After surgical implantation of optical cannulas, mice in dopamine sensor photometry experiments were individually housed. All experiments were conducted in accordance with the *National Institutes of Health Guidelines for the Use of Animals*, and all procedures approved by the Institutional Animal Care and Use Committee of the University of Pennsylvania (protocol 805643). Sample sizes are detailed in Figure legends and Data S1.

METHOD DETAILS

Stereotaxic surgery and viral injection—Specific details regarding animals used, virus delivered, and implantation are provided below for individual experiments. As described previously[2], viral injections and cannula implantations were performed on a stereotaxic frame (Kopf Instruments, Model 1900) under isoflurane anesthesia (1.5–2% + oxygen at 1 L/min) and body temperature maintained at 30°C throughout surgery (Harvard Apparatus, #50722F). Briefly, fur over the skull was removed with depilatory cream, and the skin cleaned with 70% isopropyl alcohol and betadine, after which a small anterior/posterior incision was made to expose the skull. Small (0.5 mm) holes were drilled above the target coordinates and a pulled glass needle was lowered into the injection site. DMS coordinates were AP: 0.85mm, ML: 1.25mm, DV: −2.85mm, unilaterally (dopamine sensor, anatomy) or bilaterally (all other experiments). VTA/SN coordinates were AP: - 3.00mm, ML: ±0.65mm, DV-4.40mm. 500nl (DMS) or 1000nl (VTA/SN) of specific adeno-associated virus (see individual experimental details below) was infused at 125 nl/min using a microinfusion

pump (Harvard Apparatus, #70–3007), and the injection needle was removed 10 min after termination of viral infusion. For implantation surgeries (microdialysis, dopamine sensor, microinjection), 2 small screws were secured into the skull. The implant was lowered into the injection site and held with dental cement (Den-Mat, Geristore A and B). Mice were given a minimum of 7d (microdialysis, microinjection) or 3 weeks (all other experiments) to recover from surgery prior to subsequent experimental testing.

Histological verification—After the completion of behavioral experiments, mice were deeply anesthetized with i.p. pentobarbital (Nembutal, 50 mg/ml solution) and transcardially perfused with 4% formalin/PBS followed by PBS. Following overnight storage in 4% formalin, brains were stored in 30% sucrose until fully saturated, then sectioned via vibratome (Vibratome, Model 1000plus) or cryostat (Leica Microsystems, Model CM3050S). Viral expression and implant placements were imaged on a standard epifluorescent microscope (Olympus, BX63) under 4X (Olympus, 0.16NA) or 10x (Olympus, 0.4NA) objectives.

In vivo microdialysis—The effects of LTSI inhibition on extracellular striatal dopamine were investigated using *in vivo* microdialysis. $SST^{Cre/+}$ mice (n=4) were injected with AAVDJ.EF1α.DIO.ZsGreen-T2A-Kir2.1 in one striatal hemisphere and AAV1.CAG.DIO.GFP in the other striatal hemisphere. Microdialysis guide cannulae (3mm length; Synaptech, S-3000) were aimed at the injection site and implanted at a 15° angle (AP +0.85, ML ±1.99, DV-2.31).

Mice underwent *in vivo* microdialysis after 7–10d recovery from surgery. On the night before sample collection, a microdialysis probe with 1mm active polyacrylonitrile membrane (Synaptech, S-3010) was lowered into each guide. The probe was perfused with artificial CSF (aCSF, 149mM NaCl, 2.8mM KCl, 1.6mM $CaCl_2$, 1.2mM $MgCl_2$, 0.2mM ascorbic acid, 5.4mM D-Glucose) at a flow rate of 0.5μl/min. The following morning, the flow rate was increased to 2.0μl/min 2h prior to sample collection. Samples were collected by hand into 0.2 ml PCR tubes every 10min and stored on dry ice until the end of sample collection. After 5 baseline samples, mice were injected with saline (i.p.), followed 20 min later by d-amphetamine (1.0 mg/kg, i.p.). Samples were collected for 90 min following d-amphetamine administration. Following sample collection, mice perfused and probe placements and viral expression were verified as described above.

Dialysate was stored at −80°C until dopamine was analyzed by high performance liquid chromatography (HPLC) as described previously[46]. Briefly, mobile phase (4.0mM citric acid, 3.3mM sodium dodecyl sulfate, 100mM NaH_2PO_4, 0.3mM ethylenediaminetetraacetic acid, 15% acetonitrile, 5% methanol) was pumped (ThermoScientific, Model 582) through an HR-3.2 × 80mm column (3μm particle size, ThermoScientific) connected to a Coulochem II detector. An autosampler (ThermoScientific, Model 542) mixed 9.5μl dialysate with ascorbic oxidase (Sigma-Aldrich. EC 1.10.3.3; 162 units/mg) prior to injection, and dopamine signals acquired with 501 chromatography and Chromeleon Software (ThermoScientific). Dopamine concentration was quantified by comparing peak area to external standards (0–2.5 nM).

Immunohistochemistry and confocal microscopy—To determine whether LTSIs make synaptic connections in close proximity to dopamine fibers, we unilaterally injected SST-Flp/+;DAT-Cre/+ mice (n=3) with AAVDJ.EF1α.fDIO.Synaptophysin-mRuby2 in the DMS to label LTSI terminals, and AAVDJ.EF1α.DIO.Synaptophysin-EGFP in the VTA/SN to label dopamine terminals. After 3–6 weeks of viral expression, mice were transcardially perfused with 4% formalin followed by PBS, and 50μm slices sectioned on a vibratome (Vibratome, Model 1000plus). Immunohistochemistry for tyrosine hydroxylase (TH) was performed to visualize the full extent of dopaminergic processes. Free floating sections were permeabilized in 0.6% Triton X-100 and blocked in 3% normal goat serum (NGS) in PBS for 1h. Primary antibody (mouse anti-TH, 1:4000, Immunostar #22941) was incubated overnight in 1% NGS and 0.2% Triton X-100 in PBS, followed by 2h incubation in secondary antibody (goat anti-mouse Alexa 647, 1:200, Invitrogen A-21236). Slices were then mounted and scanned on a Leica TCS SP8 STED 3X confocal with white light laser and imaged with a 40X/1,3 NA oil immersion objective. Synpatophysin-GFP puncta were excited by 490nm laser wavelength and detected with 500–545nm emission detection filter, Synpatophysin-mRuby puncta were excited by 555nm laser wavelength with 571–629 emission detection filter, and Alexa647 labeled TH fibers excited by 640nm laser wavelength with 652–746nm emission detection filter. To reduce contributions from autofluorescence and increase specificity of detection, time-gated detection using a HyD detector and time window of 0.4–6.5ns was used in all channels.

Fast scan cyclic voltammetry (FSCV)—Optically evoked dopamine [oDA] was measured using fast scan cyclic voltammetry in acute striatal slices. For all FSCV experiments, SST-Flp/+;DAT-Cre/+ mice were injected with AAV5.hSyn.DIO.hChR2(H134R)-EFYP into the VTA/SN for optogenetic control of dopamine terminals. For LTSI optogenetic inhibition experiments (n=12, Figure 1D–F), one striatal hemisphere was injected with AAVDJ.EF1α.fDIO.eNpHR3.0-EYFP and the other with AAVDJ.EF1α.fDIO-EYFP. For LTSI chemogenetic excitation experiments (n=16, Figure 1G–M), one striatal hemisphere was injected with AAVDJ.hSyn.fDIO.hM3DGq-mCherry and the other with AAVDJ.EF1α.fDIO.mRuby2. Virus was allowed to express for at least 4 weeks prior to FSCV recordings.

To obtain acute striatal slices, mice were anesthetized with isoflurane and transcardially perfused with ice-cold sucrose cutting solution (225mM sucrose, 13.9mM NaCl, 26.2mM $NaHCO_3$, 1mM NaH_2PO_4, 1.25mM glucose, 2.5mM KCl, 0.1mM $CaCl_2$, 4.9mM $MgCl_2$). The brain was removed, hemispheres bisected, and coronally sectioned (300μm) on a vibratome (Leica, Model VT1200s). Slices were incubated at 32°C for 15min in oxygenated (95% O_2, 5% CO_2) aCSF (124mM NaCl, 26.2mM $NaHCO_3$, 1mM NaH_2PO_4, 10mM glucose, 2.5mM KCl, 2.5mM $CaCl_2$, 1.3mM $MgCl_2$, 0.4mM ascorbic acid), followed by at least 1h incubation at room temperature (20–22°C) prior to recordings.

For recording, slices were placed in a recording chamber, fully submerged in oxygenated aCSF at a flow rate of 1.4–1.6 ml/min, maintained at 30–32°C. All experiments were conducted in the presence of 1μM DHβE and 1μM scopolamine to preclude any possible effects of LTSI manipulation on cholinergic transmission. Carbon fiber electrodes (Kation Scientific, #E1011–20mod CarboStar1, custom 200μm tip length, 7μm diameter) were

conditioned at 60Hz for 20 min in aCSF prior to first use. Carbon fiber electrodes were lowered 60–80μm into the DMS at a 20° angle.

To optogenetically evoke dopamine (oDA), a 2ms pulse of 470nm light was illuminated through the 40x objective (Olympus, 0.8NA water immersion). Pulses were delivered every 3min, which allowed for stable release over several hours. A light intensity that elicited approximately 50% maximal [oDA] was determined for each recording location and used for experimental stimulation. A stable baseline (<10% variability in [oDA] over 5 consecutive samples) was established prior to LTSI manipulations. The scanning voltage was a triangular waveform (−0.4 to +1.2V vs Ag/AgCl), with a scan rate of 400 V/s every 100ms using a voltammeter (Dagan Corp., CHEM-CLAMP). Raw traces of oDA were analyzed using the Demon Voltammetry software package[47].

Halorhodopsin-mediated LTSI inhibition: After a stable baseline was established (<10% variability in [oDA] across 5 consecutive samples), the effects of optogenetic LTSI inhibition were probed. Slices were illuminated with 617nm light (0.9 mW/mm^2) through the 40X objective in one of four conditions: (1) 4s 617nm illumination, with oDA stimulation at 2s, (2) 4s 617nm illumination, with oDA stimulation 500ms after 617nm termination, (3) 400ms 617nm illumination, with oDA stimulation at 200ms, (4) 400ms 617nm illumination, with oDA stimulation 500ms after 617nm termination. Five [oDA] measurements were collected and averaged, and data expressed as percent change from the average of the five baseline [oDA] measurements.

Chemogenetic-mediated LTSI excitation: The effects of LTSI excitation on oDA were probed using chemogenetic activation of hM3D-Gq expressed in LTSIs. After a stable baseline was established, clozapine-n-oxide (CNO, 10μM) was added to the recording solution. The effects of $GABA_A$ and $GABA_B$ signaling were tested in three separate experiments. After 30min of CNO application, the $GABA_A$ antagonist picrotoxin (100μM) or $GABA_B$ antagonist CGP 55845 (2μM) was applied and [oDA] recorded for another 30min. In a separate experiment, after a stable baseline was established, CGP 55845 (2μM) added to the bath, followed 30 min later by application of CNO. To replicate prior findings that $GABA_B$ agonism suppresses evoked striatal dopamine[17,48,50], after a stable baseline was established, the $GABA_B$ agonist (R)-baclofen (100μM) was applied to the bath and samples recorded for 30 min. In all experiments, data were expressed as percent change from the mean of the last 5 baseline samples.

Acute slice electrophysiology—Cell-attached recordings were used to validate chemogenetic-mediated increases in LTSI activity in slice. One striatal hemisphere of SST-Flp/+;DAT-Cre/+ mice (n=4) was injected with AAVDJ.hSyn.fDIO.mRuby2 and the other striatal hemisphere injected with AAVDJ.hSyn.fDIO.hM3DGq.mCherry.

Our general electrophysiology procedures have been described previously[2]. Briefly, mice were anesthetized with isoflurane and transcardially perfused with ice-cold aCSF (124 mM NaCl, 1.2 mM NaH_2PO_4, 2.5 mM $NaHCO_3$, 5 mM HEPES, 13 mM glucose, 1.3 mM $MgSO_4$, 2.5 mM $CaCl_2$). The brain was then quickly removed and coronally sectioned (250 μm) on a vibratome (Leica, Model VT1200s). Slices were then incubated at 32°C for

12–15min in an NMDG-based recovery solution (92 mM NMDG, 2.5 mM KCl, 1.2 mM NaH_2PO_4, 30 mM $NaHCO_3$, 20 mM HEPES, 25 mM glucose, 5 mM sodium ascorbate, 2 mM thiourea, 3 mM sodium pyruvate, 10 mM $MgSO_4$, 0.5 mM $CaCl_2$), then transferred to room temperature (20–22°C) aCSF for at least 1h before recording. For recording, slices were placed in a recording chamber, fully submerged in oxygenated (95% O_2, 5% CO_2) aCSF at a flow rate of 1.4–1.6 mL/min, and maintained at 29–30°C.

Cell-attached recordings of mRuby+ (n=10) or hM3D-mCherry+ (n=10) cells were made with electrodes filled with aCSF. We determined LTSI firing frequency (Hz) in 5 min recordings under baseline aCSF conditions to 5 min recordings in the presence of CNO (10μM). Neuronal spiking was detected by Neuromatic (v 3.0, Jason Rothman), and firing frequency was calculated as the overall spiking over the recording time window. Recordings were sampled at 20kHz and filtered at 2.8kHz. Data acquisition was in Igor 6.32 (Wavemetrics) using Recording Artist (Rick Gerkin) and analyzed offline in Igor 7.

Operant Task—Methods for our operant learning task have been described in detail previously[2]. Briefly, mice were food deprived to 85–90% of free feeding weight prior to behavioral training. Experiments were conducted in a modular operant chamber (Med Associates Inc, Model ENV307W, 21.59 × 18.08 × 12.7cm) equipped with a modified liquid reward magazine flanked by retractable levers on either side. Chocolate liquid reward (Nestlé Boost, 10μl) served as the positive reinforcer, delivered into the reward magazine by a pump (Med Associates Inc, Model PHM-100). Mice were first familiarized with the operant chambers in magazine training sessions, where 10μl reward was delivered at the onset of 10s magazine light illumination once per minute for 40min. These sessions continued for a minimum of 2 days until mice had fewer than 10 omissions (trials in which mice did not retrieve the reward within 10s of magazine light illumination).

Mice were then trained on a fixed ratio 1 (FR1) self-initiated two-choice operant task (Figure 2C). The task structured into four discrete phases: (1) Inter-trial interval (ITI) - all lights were off for 5s between each trial), (2) Initiation - magazine light illuminated, and nosepoke initiated the trial), (3) Choice - extension of both retractable levers for either 10s or until a lever was pressed. In the event of an omission (10s without press), levers were retracted and the trial ended, (4) Outcome - mice were randomly assigned a correct lever (left or right); pressing the correct lever resulted in 5s magazine light illumination and 10μl chocolate reward, ending the trial, while pressing the incorrect lever ended the trial.

Sigmoidal modeling of learning curves: Learning curves for each mouse were modeled by fitting trial accuracy over time to a sigmoidal function. For each trial, accuracy was defined as the percentage of rewarded trials in the previous ten initiated trials (including correct choice, incorrect choice, and omission). Accuracy over trials was then fit with sigm_fit from the MATLAB Central File Exchange to the sigmoidal function

$$f(x) = a + \frac{(b-a)}{1 + 10^{(\log(c) - x) * d}}$$

where a is the minimum, b is the maximum, c is the x value at half height of the function, and d is the slope. To next bin the trials into pre-learning, active learning, and post-learning periods, the maximum and minimum values of the second derivative of the function were used. These values are the inflection points of the curve, demarcating when the slope is changing direction. Learning rate was defined as the instantaneous slope of the trial at the half-height of the sigmoidal function (Figure 2D).

Fiber photometry—Mice were unilaterally injected with AAV9.hSyn.GRAB-DA2m combined with either AAVDJ.EF1α.DIO.mRuby2 (n=11) or AAVDJ.EF1α.DIO.mRuby2-Kir2.1 (n=12) into the DMS and implanted with a 400μm diameter fiberoptic cannula (0.48NA, 3–5mm length, constructed in house). Viruses were allowed to express for at least 3 weeks until stable dopamine sensor transients were observed. Mice were then food deprived and underwent reward magazine training and operant training as described above while photometric dopamine signals were recorded.

Signal Collection: Fiber photometry was performed as described previously[2]. Mice were attached via an optical fiber (400μm core, 0.48NA; Doric Lenses), which was connected to a Doric 4-port minicube (FMC4, Doric Lenses). Dual color LED light (470nm for GRAB-DA stimulation, ThorLabs #MF470F3; 405nm for artifact control fluorescence, ThorLabs #MF405FP1) was delivered through the fiberoptic cannula into the brain at 10–30μW (ThorLabs, LED Driver Model DC4104). Photon emissions were passed through a dichroic mirror and 5000–550nm cult filter, then detected by a femtowatt silicon photoreceiver (Newport, Model 2141). Analog signals were demodulated and recorded with an RZ5 processor and Synapse Software (Tucker Davis Technologies). Prior to each recording session, 470nm light was passed through the patch cord for at least 4h to reduce autofluorescence.

Mice were connected to the patch cord with the LEDs on in the operant chambers for at least 10 min prior to experimental sessions to allow for habituation. All recording sessions began with a 10 min baseline period. Operant training sessions as described above were typically 60min, but allowed to extend longer (no more than 120min) if the mouse had started to acquire the task but was not yet exhibiting consistent accurate performance.

Signal Analysis: The demodulated 470nm and 405nm signals were processed and analyzed with custom scripts written in Matlab (MathWorks, Version 2017b). Data analysis was adapted from our previously described methodology[2], with some modifications made to optimize for dopamine signal analysis. Data were down-sampled to 40Hz then digitally filtered (filtfilt in Matlab). Over extended recording sessions, there may be steady decreases in baseline autofluorescence. In order to account for this, the 470nm signal at the end of the recording was baselined to zero, the data fit to a double exponential curve, and F/F calculated as $(F-F_0)/F_0$. The Z score calculated as the difference between the ΔF/F and mean ΔF/F for the recording session, divided by the standard deviation of the ΔF/F across the recording session.

Dopamine sensor peak events were calculated using custom peak detection scripts[2,49]. A 10s moving window was used for thresholding, where high amplitude events (local maxima

greater than two median average deviations above the median of the moving window) were removed to calculate a new baseline moving median. Peaks were defined as events with local maxima greater than 3 median average deviations above this new baseline moving median. Peak amplitude was calculated as the difference between the peak maxima and the local median.

We also assessed dopamine sensor activity tied to discrete behavioral events using peri-event temporal histogram (PETH) analysis. The z-scored ΔF/F signal was aligned to time 0 for each behavioral timestamp (delivered by TTL signal from MedPC to Synapse software) and a the 2.5s before and after the timestamp were extracted. The peak z-score (minima for ITI and initiation, maxima for choice and reward retrieval signals) and location were extracted from the 1s window around the behavioral event and areas under the curve (AUC) calculated for each trace.

D2 partial agonist (aripiprazole) microinjection—$SST^{Cre/+}$ mice were bilaterally injected with either AAVDJ.EF1α.DIO.ZsGreen-Kir2.1 (n=17) or AAV1.CAG.DIO-EGFP (n=17), and implanted with bilateral microinjection cannulae (Plastics1, C235G-3.0/SPC 4mm length). Dummy cannulae with 1mm protrusion (Plastics1, 235DC/SPC) were inserted in microinjector cannulae and held in place with a dust cap (Plastics1, 303DC/1). Mice were given 7d to recover before food deprivation and operant training.

Microinjection procedure: Microinjections occurred 20 min prior to magazine and operant training sessions. Dummy cannulae were replaced with microinfusion cannulae (Plastics1, C235I/SPC 5mm, 1mm projection beyond guide) connected by PE50 tubing to an infusion pump (Harvard Apparatus, 704506 Pump 11 Pico Plus Elite). Aripiprazole (100ng/side) or vehicle was administered in a volume of 250nl/side across 2min, and injectors left in place for an additional 1min to allow for diffusion from the injection site and prevent backflow. The dose for aripiprazole was selected based on prior research[51].

To acclimate mice to microinjection procedures, all mice received vehicle (see ‘Drugs’ below) infusions prior to the three magazine training sessions. Subsequently, mice received either aripiprazole (n=8 LTSI-GFP, n=9 LTSI-Kir) or vehicle (n=9 LTSI-GFP, n=8 LTSI-Kir) prior to each 1h operant training session. Mice continued operant training until they obtained 50 rewards within one session.

Open Field: After completing operant training, a subset of mice (n=6 LTSI-GFP, n=6 LTSI-Kir) were tested in an open field to evaluate the effects of aripiprazole on general locomotor behavior. Mice were first habituated to the open field arena (15” x 15” box) placed directly underneath a ceiling-mounted camera in a one hour session. The periphery and dimensions of the arenas were defined in video tracking software (SmartScan 3.0) and total distance traveled was recorded and used for analysis. The next day, mice were randomly assigned to receive vehicle or aripiprazole microinfusion, after which they were placed in the open field arena. Recording began 20 min after the microinfusion, and distance traveled measured for 30 min. The following day, the procedure was repeated with mice receiving the opposite microinfusion.

Drugs—Dihydro-β-erythroidine (DHβE), (R)-baclofen, clozapine N oxide (CNO), and aripiprazole were obtained from Tocris Bioscience; all other chemicals were obtained from Sigma-Aldrich. Aripipirazole was dissolved in 1μl glacial acetic acid, then brought to volume with deionized water and pH adjusted to 5.2 with NaOH. The vehicle was prepared in the same way, without the addition of aripiprazole. Aripiprazole and vehicle stocks were made the same day, aliquoted, and stored at −20°C. Stock solutions for drugs used in fast scan cyclic voltammetry were prepared in deionized water (100mM DHβE, 100mM scopolamine, 100mM CGP55845) or DMSO (100mM picrotoxin, 25mM clozapine-N-oxide), aliquoted and stored at −20°C.

QUANTIFICATION AND STATISTICAL ANALYSIS

General linear mixed models were performed with SAS (SAS Institute, University Edition), and all other statistical analyses were performed with Prism software (GraphPad, version 8). Detailed statistics and sample sizes for each Figure panel can be found in Data S1. Appropriate t-tests (paired and unpaired), ANOVAs (one-way, two-way, two-way repeated measures, three-way repeated measures), and general linear mixed models (GLMM) were perform as indicated in the results and Data S1. ANOVAs/GLMMs with significant main effects/interactions were followed up with *a priori* driven post-hoc tests with Bonferroni corrections for multiple comparisons. Data that violated assumptions of normality were transformed as indicated in Data S1, and Geisser-Greenhouse corrections applied to data that violated assumptions of sphericity. Kenward-Roger corrections (KENWARDROGER2) were applied in GLMMs to correct degrees of freedom for fixed effects.

Supplementary Material

Refer to Web version on PubMed Central for supplementary material.

ACKNOWLEDGEMENTS

This work was supported by NIMH F32 MH114506 to ENH, Howard Hughes Medical Institute Gilliam Fellowship to MFD, NIMH R00MH099243, R01 MH118369, and Whitehall Foundation grants to MVF. We thank William Doyon and John Dani for HPLC use for microdialysis experiments, Deborah Kwon and Zhaolan (Joe) Zhou for assistance with the open field experiment, Emily Black, Jessica Shaw, Jung Hoon Shin, and Veronica Alvarez for assistance establishing fast scan cyclic voltammetry methodology, and Yulong Li for assistance with the GRAB-DA sensor. We thank B.K. Lim for the pAAV.EF1α.DIO.ZsGreen-T2A-Kir2.1 plasmid, Ben Arenkiel for the pAAV.EF1α.Synaptophysin-EGFP plasmid, and Theodoros Tsetsenis for the pAAV.EF1α.fDIO.NpHR3.0 plasmid that served as a backbone for generating all fDIO constructs in this paper. We also thank Nathan Henderson for initial confocal imaging pilot work, and Andrea Stout and the Cell and Developmental Biology Microscopy core at the Perelman School of Medicine for the confocal imaging presented in this paper. Finally, we thank Patrick Rothwell for constructive feedback on the manuscript draft.

REFERENCES

1. Tepper JM, Koós T, Ibanez-Sandoval O, Tecuapetla F, Faust TW, and Assous M. (2018). Heterogeneity and Diversity of Striatal GABAergic Interneurons: Update 2018. Front. Neuroanat. 12, 91. [PubMed: 30467465]
2. Holly EN, Davatolhagh MF, Choi K, Alabi OO, Vargas Cifuentes L, and Fuccillo MV (2019). Striatal Low-Threshold Spiking Interneurons Regulate Goal-Directed Learning. Neuron 103, 92–101.e6. [PubMed: 31097361]
3. Cox J, and Witten IB (2019). Striatal circuits for reward learning and decision-making. Nat. Rev. Neurosci. 20, 482–494. [PubMed: 31171839]

4. Lovinger DM (2010). Neurotransmitter Roles in Synaptic Modulation, Plasticity and Learning in the Dorsal Striatum. Neuropharmacology 58, 951–961. [PubMed: 20096294]
5. Niv Y, Daw ND, Joel D, and Dayan P. (2007). Tonic dopamine: opportunity costs and the control of response vigor. Psychopharmacology (Berl.) 191, 507–520. [PubMed: 17031711]
6. Lin C-W, Sim S, Ainsworth A, Okada M, Kelsch W, and Lois C. (2010). Genetically increased cell-intrinsic excitability enhances neuronal integration into adult brain circuits. Neuron 65, 32–39. [PubMed: 20152111]
7. Nolan SO, Zachry JE, Johnson AR, Brady LJ, Siciliano CA, and Calipari ES Direct dopamine terminal regulation by local striatal microcircuitry. J. Neurochem. n/a.
8. Brimblecombe KR, Threlfell S, Dautan D, Kosillo P, Mena-Segovia J, and Cragg SJ (2018). Targeted Activation of Cholinergic Interneurons Accounts for the Modulation of Dopamine by Striatal Nicotinic Receptors. eNeuro 5.
9. Zhou FM, Liang Y, and Dani JA (2001). Endogenous nicotinic cholinergic activity regulates dopamine release in the striatum. Nat. Neurosci. 4, 1224–1229. [PubMed: 11713470]
10. Threlfell S, Lalic T, Platt NJ, Jennings KA, Deisseroth K, and Cragg SJ (2012). Striatal Dopamine Release Is Triggered by Synchronized Activity in Cholinergic Interneurons. Neuron 75, 58–64. [PubMed: 22794260]
11. Shin JH, Adrover MF, and Alvarez VA (2017). Distinctive Modulation of Dopamine Release in the Nucleus Accumbens Shell Mediated by Dopamine and Acetylcholine Receptors. J. Neurosci. Off. J. Soc. Neurosci. 37, 11166–11180.
12. Melchior JR, Ferris MJ, Stuber GD, Riddle DR, and Jones SR (2015). Optogenetic versus electrical stimulation of dopamine terminals in the nucleus accumbens reveals local modulation of presynaptic release. J. Neurochem. 134, 833–844. [PubMed: 26011081]
13. Grace AA, and Bunney BS (1985). Opposing effects of striatonigral feedback pathways on midbrain dopamine cell activity. Brain Res. 333, 271–284. [PubMed: 2986775]
14. Cachope R, Mateo Y, Mathur BN, Irving J, Wang H-L, Morales M, Lovinger DM, and Cheer JF (2012). Selective activation of cholinergic interneurons enhances accumbal phasic dopamine release: setting the tone for reward processing. Cell Rep. 2, 33–41. [PubMed: 22840394]
15. Beatty JA, Sullivan MA, Morikawa H, and Wilson CJ (2012). Complex autonomous firing patterns of striatal low-threshold spike interneurons. J. Neurophysiol. 108, 771–781. [PubMed: 22572945]
16. Brodnik ZD, Batra A, Oleson EB, and España RA (2019). Local GABAA Receptor-Mediated Suppression of Dopamine Release within the Nucleus Accumbens. ACS Chem. Neurosci. 10, 1978–1985. [PubMed: 30253088]
17. Lopes EF, Roberts BM, Siddorn RE, Clements MA, and Cragg SJ (2019). Inhibition of Nigrostriatal Dopamine Release by Striatal GABAA and GABAB Receptors. J. Neurosci. Off. J. Soc. Neurosci. 39, 1058–1065.
18. Kramer PF, Twedell EL, Shin JH, Zhang R, and Khaliq ZM (2020). Axonal mechanisms mediating γ-aminobutyric acid receptor type A (GABA-A) inhibition of striatal dopamine release. eLife 9.
19. Hamilos AE, Spedicato G, Hong Y, Sun F, Li Y, and Assad JA (2020). Dynamic dopaminergic activity controls the timing of self-timed movement. bioRxiv, 2020.05.13.094904.
20. Krechevsky I. (1938). A study of the continuity of the problem-solving process. Psychol. Rev. 45, 107–133.
21. Heinneman EG (1983). The presolution period and detection of statistical associations. In Quantitative Analyses of Behavior: Discrimination Processes, Commons ML, Herrnstein RJ, and Wagner AR, eds. (Ballinger), pp. 21–36.
22. Chase S, Schupak C, and Ploog BO (2012). Attention, the presolution period, and choice accuracy in pigeons. Behav. Processes 89, 225–231. [PubMed: 22138233]
23. Bathellier B, Tee SP, Hrovat C, and Rumpel S. (2013). A multiplicative reinforcement learning model capturing learning dynamics and interindividual variability in mice. Proc. Natl. Acad. Sci. 110, 19950–19955. [PubMed: 24255115]
24. Skinner BF (1950). Are theories of learning necessary? Psychol. Rev. 57, 193–216. [PubMed: 15440996]

25. Parker NF, Cameron CM, Taliaferro JP, Lee J, Choi JY, Davidson TJ, Daw ND, and Witten IB (2016). Reward and choice encoding in terminals of midbrain dopamine neurons depends on striatal target. Nat. Neurosci. 19, 845–854. [PubMed: 27110917]
26. Barter JW, Li S, Lu D, Bartholomew RA, Rossi MA, Shoemaker CT, Salas-Meza D, Gaidis E, and Yin HH (2015). Beyond reward prediction errors: the role of dopamine in movement kinematics. Front. Integr. Neurosci. 9, 39. [PubMed: 26074791]
27. Ito H, Takano H, Arakawa R, Takahashi H, Kodaka F, Takahata K, Nogami T, Suzuki M, and Suhara T. (2012). Effects of dopamine D2 receptor partial agonist antipsychotic aripiprazole on dopamine synthesis in human brain measured by PET with L-[β−11C]DOPA. PloS One 7, e46488.
28. Burris KD, Molski TF, Xu C, Ryan E, Tottori K, Kikuchi T, Yocca FD, and Molinoff PB (2002). Aripiprazole, a Novel Antipsychotic, Is a High-Affinity Partial Agonist at Human Dopamine D2 Receptors. J. Pharmacol. Exp. Ther. 302, 381–389. [PubMed: 12065741]
29. Assous M, Kaminer J, Shah F, Garg A, Koós T, and Tepper JM (2017). Differential processing of thalamic information via distinct striatal interneuron circuits. Nat. Commun. 8, 15860. [PubMed: 28604688]
30. Assous M, Faust TW, Assini R, Shah F, Sidibe Y, and Tepper JM (2018). Identification and Characterization of a Novel Spontaneously Active Bursty GABAergic Interneuron in the Mouse Striatum. J. Neurosci. 38, 5688–5699. [PubMed: 29789374]
31. Condon MD, Platt NJ, Zhang Y-F, Roberts BM, Clements MA, Vietti-Michelina S, Tseu M-Y, Brimblecombe KR, Threlfell S, Mann EO, et al. (2019). Plasticity in striatal dopamine release is governed by release-independent depression and the dopamine transporter. Nat. Commun. 10.
32. Mohebi A, Pettibone JR, Hamid AA, Wong J-MT, Vinson LT, Patriarchi T, Tian L, Kennedy RT, and Berke JD (2019). Dissociable dopamine dynamics for learning and motivation. Nature 570, 65–70. [PubMed: 31118513]
33. Mohebi A, and Berke JD (2020). Dopamine release drives motivation, independently from dopamine cell firing. Neuropsychopharmacol. Off. Publ. Am. Coll. Neuropsychopharmacol. 45, 220.
34. Trulson ME (1985). Simultaneous recording of substantia nigra neurons and voltammetric release of dopamine in the caudate of behaving cats. Brain Res. Bull. 15, 221–223. [PubMed: 4041929]
35. Rice ME, Patel JC, and Cragg SJ (2011). Dopamine release in the basal ganglia. Neuroscience 198, 112–137. [PubMed: 21939738]
36. Sulzer D, Cragg SJ, and Rice ME (2016). Striatal dopamine neurotransmission: Regulation of release and uptake. Basal Ganglia 6, 123–148. [PubMed: 27141430]
37. Berke JD (2018). What does dopamine mean? Nat. Neurosci. 21, 787–793. [PubMed: 29760524]
38. Straub C, Saulnier JL, Bègue A, Feng DD, Huang KW, and Sabatini BL (2016). Principles of Synaptic Organization of GABAergic Interneurons in the Striatum. Neuron 92, 84–92. [PubMed: 27710792]
39. Elghaba R, Vautrelle N, and Bracci E. (2016). Mutual Control of Cholinergic and Low-Threshold Spike Interneurons in the Striatum. Front. Cell. Neurosci. 10, 111. [PubMed: 27199665]
40. Frost Nylén J, Carannante I, Grillner S, and Hellgren Kotaleski J. (2020). Reciprocal interaction between striatal cholinergic and low-threshold spiking interneurons - A computational study. Eur. J. Neurosci.
41. Melendez-Zaidi AE, Lakshminarasimhah H, and Surmeier DJ (2019). Cholinergic modulation of striatal nitric oxide-producing interneurons. Eur. J. Neurosci. 50, 3713–3731. [PubMed: 31340071]
42. Choi K, Holly EN, Davatolhagh MF, Beier KT, and Fuccillo MV (2019). Integrated anatomical and physiological mapping of striatal afferent projections. Eur. J. Neurosci. 49, 623–636. [PubMed: 29359830]
43. Cains S, Blomeley CP, and Bracci E. (2012). Serotonin inhibits low-threshold spike interneurons in the striatum. J. Physiol. 590, 2241–2252. [PubMed: 22495583]
44. Fisher SD, Robertson PB, Black MJ, Redgrave P, Sagar MA, Abraham WC, and Reynolds JNJ (2017). Reinforcement determines the timing dependence of corticostriatal synaptic plasticity in vivo. Nat. Commun. 8, 334. [PubMed: 28839128]

45. Fino E, Vandecasteele M, Perez S, Saudou F, and Venance L. (2018). Region-specific and state-dependent action of striatal GABAergic interneurons. Nat. Commun. 9, 3339. [PubMed: 30131490]

46. Doyon WM, Dong Y, Ostroumov A, Thomas AM, Zhang TA, and Dani JA (2013). Nicotine decreases ethanol-induced dopamine signaling and increases self-administration via stress hormones. Neuron 79, 530–540. [PubMed: 23871233]

47. Yorgason JT, España RA, and Jones SR (2011). Demon voltammetry and analysis software: analysis of cocaine-induced alterations in dopamine signaling using multiple kinetic measures. J. Neurosci. Methods 202, 158–164. [PubMed: 21392532]

48. Schmitz Y, Schmauss C, and Sulzer D. (2002). Altered Dopamine Release and Uptake Kinetics in Mice Lacking D2 Receptors. J. Neurosci. 22, 8002–8009. [PubMed: 12223553]

49. Muir J, Lorsch ZS, Ramakrishnan C, Deisseroth K, Nestler EJ, Calipari ES, and Bagot RC (2018). In Vivo Fiber Photometry Reveals Signature of Future Stress Susceptibility in Nucleus Accumbens. Neuropsychopharmacology 43, 255–263. [PubMed: 28589967]

50. Pitman KA, Puil E, and Borgland SL (2014). GABAB modulation of dopamine release in the nucleus accumbens core. Eur. J. Neurosci. 40, 3472–3480. [PubMed: 25229321]

51. Besson M, Belin D, McNamara R, Theobald DE, Castel A, Beckett VL, Crittenden BM, Newman AH, Everitt BJ, Robbins TW, et al. (2010). Dissociable Control of Impulsivity in Rats by Dopamine D2/3 Receptors in the Core and Shell Subregions of the Nucleus Accumbens. Neuropsychopharmacology 35, 560–569. [PubMed: 19847161]

Highlights

- Striatal low-threshold spiking interneurons (LTSIs) synapse near dopamine terminals
- *In vitro,* LTSIs directly and locally reduce striatal dopamine via $GABA_B$ signaling
- *In vivo*, LTSIs strongly modulate striatal dopamine dynamics during operant learning
- Local D2 partial agonism suggests LTSI-dopamine interactions underlie learning

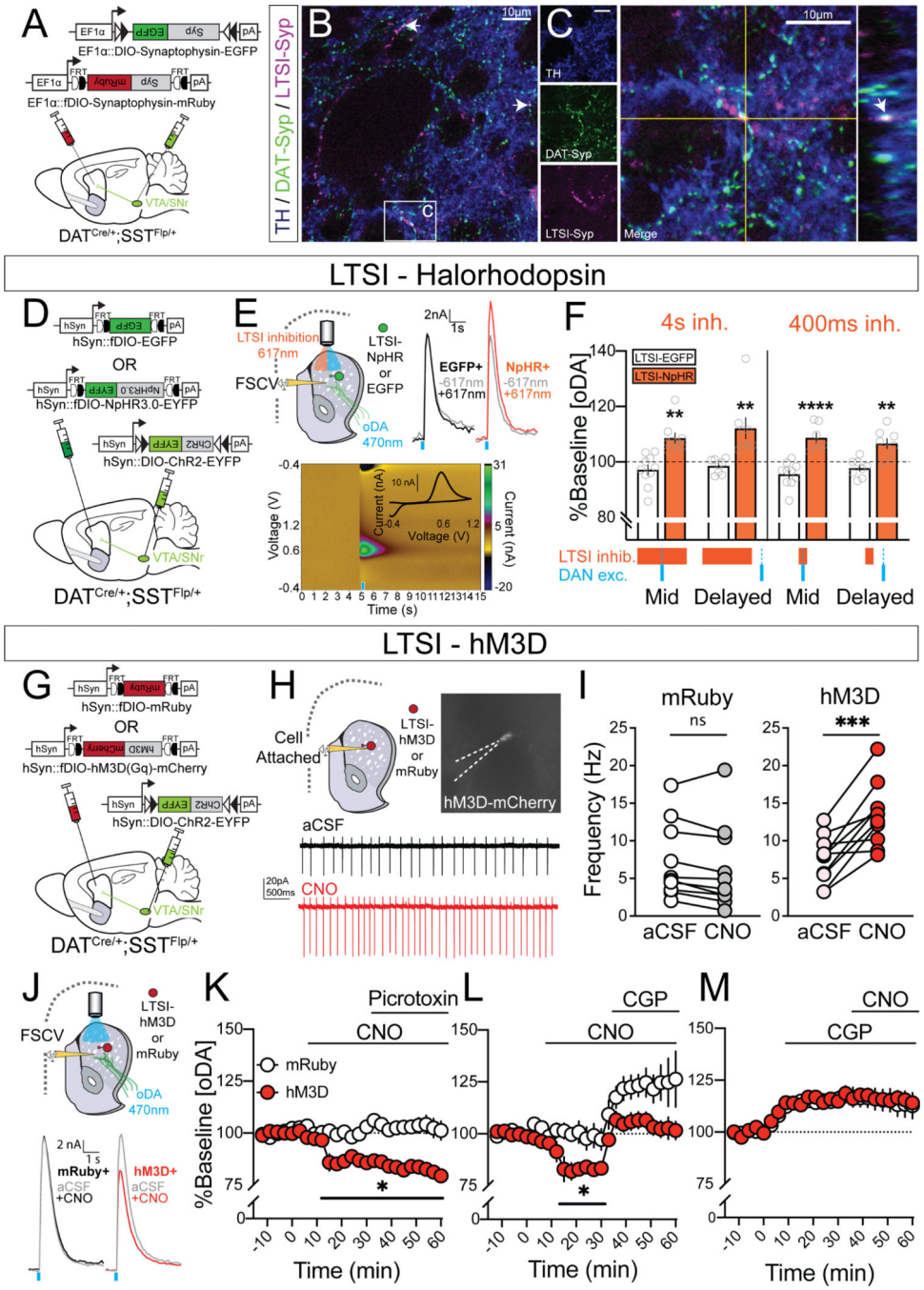

Figure 1. LTSIs attenuate optogenetically evoked dopamine via $GABA_B$ signaling.

(A) Experimental design for Synaptophysin (Syp) labeling of LTSI (SST-Flp+) and dopaminergic (DAT-Cre+) terminals. (B) Representative 20X image demonstrating multiple points of colocalization indicated by white arrows between DAT-Syp (green), LTSI-Syp (magenta), and tyrosine hydroxylase (TH) immunoreactivity (blue). (C) 40X image of colocalization indicated by arrow C in (B); orthogonal YZ view shown on right with colocalization point marked by white arrow. (D) Experimental design for optogenetically driven LTSI inhibition and dopamine terminal excitation. (E) Recording schematic (top

left), sample traces (top right) and voltammogram (bottom) for acute slice fast scan cyclic voltammetry (FSCV) experiments testing the effect of LTSI inhibition on optogenetically-evoked dopamine (oDA). (F) Percent change from baseline oDA in striatal slices with LTSIs expressing EGFP (white) or halorhodopsin (NpHR, orange). oDA was evoked by 2ms 470nm light stimulation in the middle ('Mid') or 500ms after termination ('Delayed') of 4s (left) or 400ms (right) 617nm light stimulation.: 4s sample sizes: LTSI-EGFP 'Mid' n=10 slices / 5 mice, 'Delayed' n=8 slices / 5 mice; LTSI-NpHR 'Mid' n=9 slices / 5 mice, 'Delayed' n=8 slices / 5 mice; 400ms sample sizes: LTSI-EGFP 'Mid' n=10 slices / 5 mice, 'Delayed' n=8 slices / 4 mice; LTSI-NpHR 'Mid' n=7 slices / 5 mice, 'Delayed' n=8 slices / 4 mice. **p<0.01, **** p<0.00001 vs LTSI-EGFP control in same stimulation condition. Data expressed as mean ± SEM, with individual values shown in gray. (G) Experimental design for chemogenetic LTSI excitation and optogenetic dopamine terminal excitation. (H) Recording schematic and sample traces for cell-attached electrophysiological recordings. (I) Spontaneous firing frequency (Hz) in mRuby+ (left; n=10 cells / 4 mice) and hM3D+ (right; n=10 cells / 4 mice) LTSIs in the presence of aCSF and clozapine-N-oxide (CNO, 10μM). **p<0.01 pairwise comparison of firing frequency. (J) Recording schematic and sample traces for acute slice FSCV experiments testing the effect of LTSI excitation on oDA. (K) Effects of $GABA_A$ antagonism on oDA suppression caused by chemogenetic LTSI excitation. CNO (10μM) was applied after a stable baseline (<10% variability in 5 consecutive oDA stimulations), and picrotoxin (100μM) was added 30min later on slices where LTSIs expressed mRuby (n=7) or hM3D (n=8). *p<0.05 vs baseline. Data expressed as mean ± SEM. (L,M) Effects of $GABA_B$ antagonism on oDA suppression caused by chemogenetic LTSI excitation. The $GABA_B$ antagonist CGP55845 (2μM) was applied (L) 30min after CNO or (M) was present in the recording solution during baseline sample collection prior to CNO application (right). *p<0.05 vs baseline. Data expressed as mean ± SEM. See Data S1A for detailed sample sizes and statistics, and see also related Figure S1.

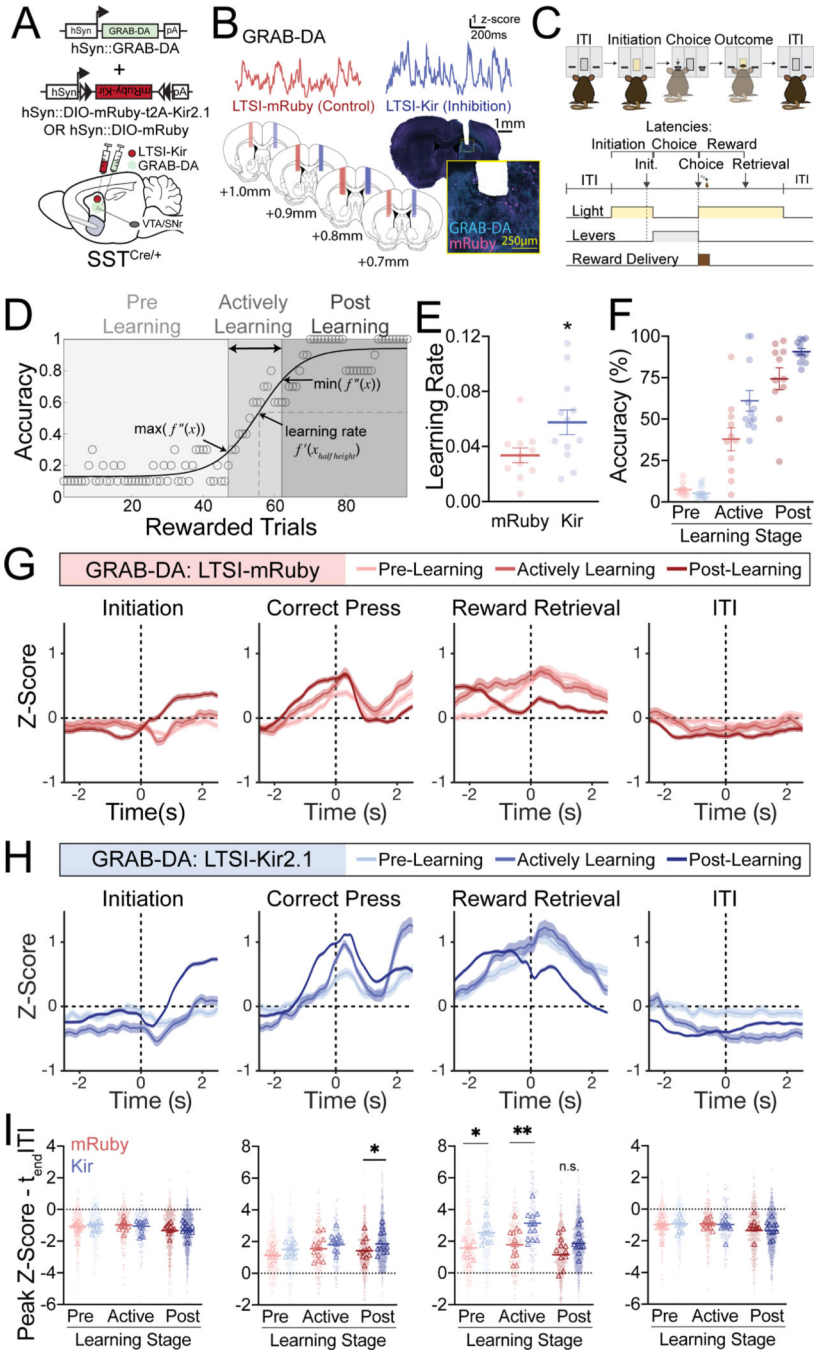

Figure 2. LTSI inhibition amplifies dopamine signaling and accelerates operant learning.

(A) Experimental design for recording dopamine signals with or without LTSI inhibition during operant learning. (B) Sample GRAB-DA dopamine sensor traces (top) and fiberoptic cannula placement (bottom). (C) Self-initiated operant task. (D) Sigmoidal modeling of learning. For each trial, accuracy was calculated as the number of correct presses in the preceding 10 initiated trials. Only rewarded trials are depicted for simplification. The inflection points of the sigmoidal function (maximum and minimum values of the second derivative) were used to bin trials into ‘pre-learning’, ‘actively learning’, and ‘post-learning’

periods. The learning rate was defined as the instantaneous slope at the half height of the function. (E) Learning rate in mice with LTSI inhibition (Kir, n=12) or control (mRuby, n=11). *p<0.05 vs LTSI-mRuby control. (F) Accuracy in pre-learning, active learning, and post-learning periods. Two-way repeated measures ANOVA: virus p<0.05, learning stage p<0.001, interaction p<0.01. (G) Peri-event temporal histograms (PETHs) for initiations, correct presses, reward retrievals, and ITIs of pre-learning, actively learning, and post-learning trials for LTSI-mRuby control mice (n=11). Dashed vertical lines at time 0 indicate the timestamp of the behavioral event. (H) PETHs for LTSI-Kir mice (n=12). (I) Difference between peak Z-scores (minima for initiation and ITI, maxima for correct press and reward retrieval) in the 1s window surrounding each behavioral event and the signal at the end of the ITI. *p<0.05, ***p<0.001 vs mRuby control at same learning stage. Lines in dot plots represent means; dots represent individual trials and open triangles represent animal means. All PETH data represented as mean ± SEM. See Data S1B for detailed statistics, and see also related Figures S1 and S2.

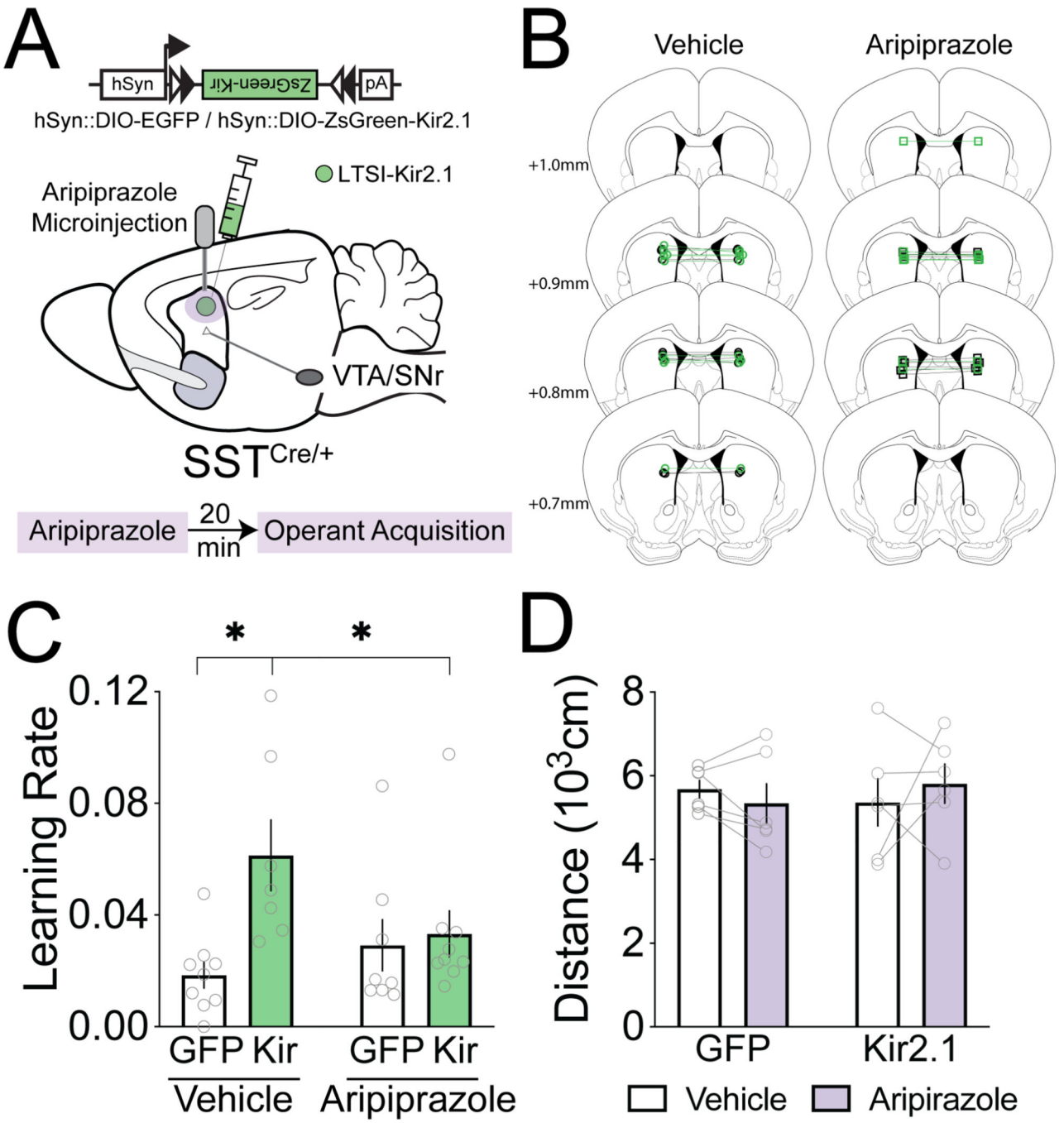

Figure 3. Intra-striatal dopamine D2 partial agonism prevents the effects of LTSI inhibition on learning.

(A) Experimental design. Aripiprazole (100 ng/side) or vehicle was bilaterally microinjected into the dorsomedial striatum of mice with or without Kir-mediated LTSI inhibition prior to operant task acquisition sessions. (B) Placements of microinjector tips in the dorsomedial striatum. Vehicle (left): n=9 LTSI-EGFP (black circles), n=8 LTSI-Kir2.1 (green circles); Aripiprazole (right): n=8 LTSI-EGFP (black squares), n=9 LTSI-Kir2.1 (green squares). (C) Learning rate. $P<0.05$ vs Vehicle-Kir. (D) Distance traveled in an open field in a subset of LTSI-GFP (n=6) and LTSI-Kir (n=6) expressing mice one week after operant acquisition.

All data represented as mean ± SEM. See Data S1C for detailed statistics, and see also related Figure S3.

KEY RESOURCES TABLE

REAGENT or RESOURCE	SOURCE	IDENTIFIER
Antibodies		
mouse anti-Tyrosine Hydroxylase	Immunostar	Cat#22941
goat anti-mouse Alexa 647	Invitrogen	Cat#A-21236
Bacterial and Virus Strains		
AAVDJ.EF1α.DIO.ZsGreen-T2A-Kir2.1	Fuccillo Lab	N/A
AAV1.CAG.DIO.EGFP	UNC Vector Core	N/A
AAVDJ.EF1α.fDIO.Synaptophysin-mRuby2	Fuccillo Lab	N/A
AAVDJ.EF1α.DIO.Synaptophysin-EGFP	Fuccillo Lab	N/A
AAV5.hSyn.DIO.hChR2(H134R)-EFYP	UNC Vector Core	N/A
AAVDJ.EF1α.fDIO.eNpHR3.0-EYFP	Fuccillo Lab	N/A
AAVDJ.EF1α.fDIO-EYFP	Fuccillo Lab	N/A
AAVDJ.hSyn.fDIO.hM3DGq-mCherry	Stanford Virus Core	Cat#AAV-153
AAVDJ.EF1α.fDIO.mRuby2	Fuccillo Lab	N/A
AAV9.hSyn.GRAB-DA2m	Vigene	Cat#YL10013
AAVDJ.EF1α.DIO.mRuby2	Fuccillo Lab	N/A
AAVDJ.EF1α.DIO.mRuby2-Kir2.1	Fuccillo Lab	N/A
Chemicals, Peptides, and Recombinant Proteins		
Dihydro-β-erythroidine (DHβE)	Tocris Bioscience	Cat#2349
Aripiprazole	Tocris Bioscience	Cat#5584
(R)-Baclofen	Tocris Bioscience	Cat#0796
CGP55845	Sigma-Aldrich	Cat#SML0594
Clozapine N-oxide	Tocris Bioscience	Cat#4936
Scopolamine hydrobromide	Sigma-Aldrich	Cat#795437
Picrotoxin	Sigma-Aldrich	Cat#P1675
d-Amphetamine	Sigma-Aldrich	Cat#A5880
Experimental Models: Organisms/Strains		
Mouse: $Sst^{tm2.1(cre)Zjh}$/J (SST-ires-Cre)	Jackson Laboratory	Cat#013044, RRID:IMSR_JAX:013044
Mouse: $Sst^{tm3.1(flop)Zjh}$/J (SST-ires-Flp)	Jackson Laboratory	Cat#028579, RRID:IMSR_JAX:028579
Mouse: *Slc6a3*$^{tm1.1(cre)Bkmn}$/J (DAT-IRES-Cre)	Jackson Laboratory	Cat#006660, RRID:ISMR_JAX:006660
Recombinant DNA		
pAAV.EF1α.DIO.ZsGreen-T2A-Kir2.1	Byungkook Lim	N/A
pAAV.EF1α.fDIO.Synaptophysin-mRuby2	Fuccillo Lab	N/A
pAAV.EF1α.DIO.Synaptophysin-EGFP	Benjamin Arenkiel	N/A
pAAV.EF1α.fDIO.eNpHR3.0-EYFP	Theodoros Tsetsenis	N/A
pAAV.EF1α.fDIO-EYFP	Fuccillo Lab	N/A
pAAV.EF1α.fDIO.mRuby2	Fuccillo Lab	N/A
pAAV.EF1α.DIO.mRuby2	Fuccillo Lab	N/A

REAGENT or RESOURCE	SOURCE	IDENTIFIER
pAAV.EF1α.DIO.mRuby2-Kir2.1	Fuccillo Lab	N/A
Software and Algorithms		
Original code for photometry analysis	Fuccillo-lab github site	DOI: 10.5281/zenodo.5026745